

MPG–VT–UR 81/96

Critical Scattering and Two Photon Spectra for a Quark/Meson Plasma

P. Rehberg

*Institut für Theoretische Physik, Universität Heidelberg,
Philosophenweg 19, D-69120 Heidelberg, Germany*

Yu. L. Kalinovsky* and D. Blaschke

*MPG Arbeitsgruppe “Theoretische Vielteilchenphysik”,
Universität Rostock, D-18051 Rostock, Germany*

Abstract

At the Mott transition of a quark/meson plasma, mesons become unbound. This leads to the effect of critical scattering, which is studied by investigating photon pair production due to the process $q\bar{q} \rightarrow \gamma\gamma$. This process can proceed either via direct annihilation or via the formation of a mesonic resonance. It is shown that the latter channel leads to an enhancement of photon pairs with invariant mass equal to the thermal pion mass. The size of this effect measures the time the temperature stays near the Mott temperature during the evolution. It is particularly pronounced for a first order phase transition. The $\pi^0 \rightarrow \gamma\gamma$ decay gives a strong background contribution and may make the observation of critical scattering in two-photon spectra of present day heavy ion collision experiments difficult.

PACS numbers: 05.70.Jk, 12.38.Mh, 13.40.-f, 25.75.-q

*Present address: *Joint Institute for Nuclear Research, Bogoliubov Theoretical Laboratory, 141980, Dubna, Moscow region, Russia*

I. INTRODUCTION

In ultrarelativistic heavy ion collision experiments at CERN SPS and BNL AGS hadronic matter is produced under extreme conditions of temperature and density. These conditions might be sufficient for the transition to a new phase of matter, the quark gluon plasma [1,2]. Up to now, no unambiguous signature of this hypothetical phase has been found, and it appears that a rather complex analysis of observables has to be performed. The inputs for such a numerical analysis should be provided from effective approaches to QCD in the nonperturbative low energy sector where chiral symmetry breaking and confinement of QCD degrees of freedom are the prominent features.

Although plagued with nonrenormalizability and the absence of confinement, the Nambu-Jona-Lasinio (NJL) model [3–6] has been developed recently beyond the applications for calculation of hadronic mass spectra towards a kinetic description of hadronic matter at the quark-hadron phase transition [7,8]. A particularly interesting problem within this context is the description of hadrons as bound states of quarks and antiquarks and their dissolution at finite temperature and density due to thermal excitation or to compression, i. e. the Mott effect [9]. At temperatures below the Mott temperature T_M , the model contains massive constituent quarks and bound state mesons as degrees of freedom. For temperatures above T_M , these bound states dissolve and become resonant (nonperturbative) correlations. Whereas the appearance of free quarks at $T < T_M$ is an artifact of the NJL model, the situation for $T \geq T_M$ is fairly realistic, except for the absence of gluons. We thus apply the model for the description of mesonic correlations at $T \geq T_M$. It has been argued elsewhere [9,10] that the Mott transition leads to the effect of critical scattering and may have experimental consequences. In this work, we investigate the influence of such correlations in a quark plasma on the two-photon spectrum which is one of the observables measured in nucleus-nucleus collisions, see e. g. [11], and which has been previously studied in Refs. [12,13]. To this end, we present a model study of the process $q\bar{q} \rightarrow \gamma\gamma$ employing the two flavor NJL model. In the s -channel, this process proceeds via the formation of a virtual meson. At the Mott temperature, this meson becomes unbound, which leads to a divergent scattering length. We estimate the magnitude of this critical scattering effect and its sensitivity to the order

of the phase transition by comparing the spectra containing resonance contributions with those, which only contain contributions of direct annihilation. However, we give only a crude estimate of the contributions from π^0 decay into photons after freezeout.

Since presently no consistent transport theory modeling the chiral phase transition is available, we apply a hydrodynamical scenario in order to obtain the total photon spectra. In this approach, we use a model equation of state [14,15] which interpolates smoothly between a first and a second order phase transition. The results of our investigation show that the yield of photon pairs with invariant mass $m_\pi(T_M)$ depends strongly on the time the temperature stays near the critical temperature.

This paper is structured as follows: The calculation of photon production cross sections including resonance contributions is performed in Section II. In Section III we apply the Bjorken hydrodynamical expansion scenario [16] in order to calculate the invariant mass spectrum of photon pairs from a hadronizing quark plasma. In Section IV, we summarize and present the conclusions.

II. PHOTON PRODUCTION CROSS SECTIONS

A. Review of Formalism

For the calculation of photon production cross sections we employ the Nambu–Jona-Lasinio (NJL) model in its $SU_f(2)$ version [5,6]. The Lagrangian for this model reads

$$\mathcal{L} = \bar{\psi}(i\cancel{\partial} - m_{0q})\psi + G \left[(\bar{\psi}\psi)^2 + (\bar{\psi}i\gamma_5\vec{\tau}\psi)^2 \right] \quad . \quad (2.1)$$

Here G is a coupling constant of dimension MeV^{-2} and $\vec{\tau}$ the Pauli matrices in flavor space. The quark wave function ψ carries flavor and color degrees of freedom, which are implicitly summed in Eq. (2.1). The symbol m_{0q} denotes the current quark mass, which explicitly breaks chiral invariance.

The masses of the constituent quarks are computed in leading order in an expansion in the inverse number of colors, $1/N_c$ [17]. For the constituent quark masses, this corresponds to a Hartree approximation. One obtains the gap equation for the physical masses

$$m_q = m_{0q} + 4iGN_c \text{tr}_\gamma S(x, x) = m_{0q} - \frac{GN_c}{\pi^2} m_q A(m_q) \quad , \quad (2.2)$$

where the function $A(m_q)$ is given in the imaginary time Matsubara formalism [18] as

$$A(m_q) = \frac{16\pi^2}{\beta} \sum_n e^{i\omega_n \eta} \int_{|\vec{p}| < \Lambda} \frac{d^3 p}{(2\pi)^3} \frac{1}{(i\omega_n)^2 - E^2} \quad . \quad (2.3)$$

Here we have abbreviated $E = \sqrt{\vec{p}^2 + m_q^2}$, and $\omega_n = (2n + 1)\pi/\beta$ is the fermionic Matsubara frequency. The symbol $\beta = 1/T$ denotes the inverse temperature. The function $A(m_q)$ is given explicitly by [19]

$$A(m_q) = -4 \int_0^\Lambda dp \frac{p^2}{E} \tanh(\beta E/2) \quad , \quad (2.4)$$

where we have used an $O(3)$ cutoff to make the integral finite.

Mesonic correlations in the pseudoscalar (pion) and scalar (sigma) channels of the $q\bar{q}$ interaction are treated in the random phase approximation [5]. This leads to the form

$$\mathcal{D}_\pi(k_0, \vec{k}) = \frac{2G}{1 - 4G\Pi^P(k_0, \vec{k})} \quad (2.5)$$

for the pion propagator and

$$\mathcal{D}_\sigma(k_0, \vec{k}) = \frac{2G}{1 - 4G\Pi^S(k_0, \vec{k})} \quad , \quad (2.6)$$

for the σ propagator. In Eqs. (2.5) and (2.6), Π^P and Π^S denote the irreducible pseudoscalar and scalar polarization functions, respectively. They are given explicitly by [8]

$$\Pi^P(k_0, \vec{k}) = -\frac{N_c}{8\pi^2} \left[2A(m_q) - (k_0^2 - \vec{k}^2) B_0(k_0, \vec{k}) \right] \quad (2.7)$$

$$\Pi^S(k_0, \vec{k}) = -\frac{N_c}{8\pi^2} \left[2A(m_q) + (4m_q^2 - k_0^2 + \vec{k}^2) B_0(k_0, \vec{k}) \right] \quad , \quad (2.8)$$

where the function $B_0(k_0, \vec{k})$ is defined as the analytical continuation of

$$B_0(i\nu_m, \vec{k}) = \frac{16\pi^2}{\beta} \sum_n e^{i\omega_n \eta} \int_{|\vec{p}| < \Lambda} \frac{d^3 p}{(2\pi)^3} \frac{1}{[(i\omega_n)^2 - E^2]} \frac{1}{[(i\omega_n - i\nu_m)^2 - E'^2]} \quad (2.9)$$

to real values of $i\nu_m \rightarrow k_0$. In Eq. (2.9), we have used the notation $E' = \sqrt{(\vec{p} - \vec{k})^2 + m_q^2}$. In the following, we will need the function B_0 for the special case $\vec{k} = 0$, where it can be expressed as [19]

$$B_0(k_0, \vec{0}) = 8\mathcal{P} \int_0^\Lambda dp \frac{p^2 \tanh(\beta E/2)}{E[4E^2 - k_0^2]} \quad (2.10)$$

$$+ i\pi \sqrt{1 - \frac{4m_q^2}{k_0^2}} \tanh\left(\frac{\beta k_0}{4}\right) \Theta(k_0 - 2m_q) \Theta\left(2\sqrt{\Lambda^2 + m_q^2} - k_0\right) .$$

One can immediately see from this form, that $B_0(k_0, \vec{0})$ is a real function for $k_0 < 2m_q$ and a complex function for $k_0 > 2m_q$.

The masses of the π and σ mesons are obtained via the dispersion relations [5]

$$1 - 4G\Pi^P(\tilde{m}_\pi, \vec{0}) = 0 \quad (2.11)$$

$$1 - 4G\Pi^s(\tilde{m}_\sigma, \vec{0}) = 0 . \quad (2.12)$$

Note that these are in general complex equations and the solution may contain a nonzero width:

$$\tilde{m}_\alpha = m_\alpha - \frac{i}{2}\Gamma_\alpha \quad , \quad \alpha = \pi, \sigma . \quad (2.13)$$

In this case, the function $B_0(k_0, \vec{0})$ has to be analytically continued to complex values of k_0 [9]. However, Eq. (2.11) at low temperatures has *real* (bound state) solutions for \tilde{m}_π with $m_\pi(T) < 2m_q(T)$. At the Mott temperature T_M , one obtains $m_\pi(T_M) = 2m_q(T_M)$. For higher temperatures, the pion becomes a resonant state. Further details about this transition can be found in Ref. [9]. The sigma meson differs from the pion in that it is a resonance for all temperatures. In Fig. 1, we show the result of a numerical solution of Eqs. (2.2), (2.11) and (2.12), using the parameter set $m_{0q} = 5.0$ MeV, $\Lambda = 653.3$ MeV and $G\Lambda^2 = 2.105$, as a function of temperature. At low temperatures, the pion mass, which is indicated by the solid line, lies below the mass of its constituents, which is given by the dashed line. At $T = T_M$, one obtains $m_\pi(T_M) = 2m_q(T_M)$, and the pion moves from being a bound state to a resonant state. For our parameter set, this happens at $T_M = 205$ MeV. The mass of the sigma meson, which is indicated by the dotted line in Fig. 1, is larger than $2m_q$ in the whole temperature range. The sigma meson is thus a resonant state at all temperatures.

B. Photon Production Cross Sections

The Feynman diagrams, which contribute to the process $q\bar{q} \rightarrow \gamma\gamma$ in lowest order in $1/N_c$ are shown in Fig. 2. Beside the direct terms, i. e. those which do not contain resonance contributions and which are already present in quantum electrodynamics [20], there are four diagrams, in which the incoming quarks first form a virtual π^0 or σ state, which afterwards decays into two photons. We write the transition amplitude for the t -channel direct term shown in Fig. 2a as

$$-i\mathcal{M}_t = \delta_{c_1, c_2} \bar{v}_2(p_2) (-iq_f e \not{\epsilon}_2) \frac{i}{\not{p}_1 - \not{k}_1 - m_q} (-iq_f e \not{\epsilon}_1) u(p_1) . \quad (2.14)$$

In this equation, p_1 and p_2 denote the four-momenta of the incoming quarks, k_1 and k_2 the four-momenta of the outgoing photons and ϵ_1 and ϵ_2 their respective polarization vectors. The electron charge magnitude is denoted by e , q_f is the quark charge factor; one has $q_u = +2/3$ for up quarks and $q_d = -1/3$ for down quarks. The Kronecker symbol δ_{c_1, c_2} guarantees that only color singlet states can annihilate into two photons. The transition amplitude for the u -channel direct graph is evaluated analogously to be

$$-i\mathcal{M}_u = \delta_{c_1, c_2} \bar{v}_2(p_2) (-iq_f e \not{\epsilon}_1) \frac{i}{\not{p}_1 - \not{k}_2 - m_q} (-iq_f e \not{\epsilon}_2) u(p_1) . \quad (2.15)$$

Multiple rescattering in the initial state leads to the formation of a strong correlation in the s -channel as is shown diagrammatically in Fig. 2b where the correlation is described by a meson propagator. The transition amplitude corresponding to sigma propagation in the s -channel can be written as

$$-i\mathcal{M}_{s,\sigma} = \delta_{c_1, c_2} \bar{v}(p_2) u(p_1) \left[i\mathcal{D}_\sigma(\sqrt{s}, \vec{0}) \right] \left[-ia(s)(k_1^\lambda k_2^\rho - g^{\rho\lambda} k_1 k_2) \right] \epsilon_{1\rho} \epsilon_{2\lambda} . \quad (2.16)$$

In this expression, we have restricted ourselves to the kinematical situation that the center of mass system rests with respect to the medium. The factor $-ia(s)(k_1^\lambda k_2^\rho - g^{\rho\lambda} k_1 k_2)$ stems from the triangle part of the diagram in Fig. 2b. The explicit form of $a(s)$ is derived in Appendix A. Here we only note that $a(s)$ contains a factor $(1 - 4m_q^2/s)$, which leads to a suppression of this diagram near threshold. The transition amplitude corresponding to the propagation of a pionic mode is given by

$$-i\mathcal{M}_{s,\pi} = \delta_{c_1, c_2} \bar{v}(p_2) (i\gamma_5 \tau_{ff}^3) u(p_1) \left[i\mathcal{D}_\pi(\sqrt{s}, \vec{0}) \right] \left[-ib(s)\varepsilon^{\mu\nu}{}_{\lambda\rho} k_1^\lambda k_2^\rho \right] \epsilon_{1\mu} \epsilon_{2\nu} , \quad (2.17)$$

where the triangle contributions are contained in the factor $-ib(s)\varepsilon^{\mu\nu}{}_{\lambda\rho}k_1^\lambda k_2^\rho$. Here, ε denotes the totally antisymmetric tensor. As was the case for $a(s)$, an explicit expression for $b(s)$ is given in Appendix A. Compared to Eq. (2.16), this expression also contains an additional isospin factor τ_{ff}^3 , which is equal to +1 for up quarks, and -1 for down quarks in the initial state.

The integrated cross section is given by

$$\sigma_{q\bar{q}\rightarrow\gamma\gamma}(s, T) = \frac{1}{16\pi s(s - 4m_q^2)} \int_{t_{\min}}^{t_{\max}} dt \overline{|\mathcal{M}|^2} \quad , \quad (2.18)$$

where

$$\overline{|\mathcal{M}|^2} = \frac{1}{4N_c^2} \sum_{s,c} |\mathcal{M}_t + \mathcal{M}_u + \mathcal{M}_{s,\sigma} + \mathcal{M}_{s,\pi}|^2 \quad (2.19)$$

is the spin and color averaged square of the transition amplitude and the integration limits are given by

$$t_{\min} = m_q^2 - \frac{s}{2} \quad t_{\max} = t_{\min} + \frac{1}{2}\sqrt{s(s - 4m_q^2)} \quad . \quad (2.20)$$

Explicit expressions for $\overline{|\mathcal{M}|^2}$ and its integral over t can be found in Appendix B.

At the Mott temperature, the pion appearing in the s -channel graph of Fig. 2(b) switches from a bound to a resonant state. It is a well known fact from scattering theory, that a bound state at threshold leads to a divergent scattering length. In the present calculation, this can be shown explicitly by noticing that the pion propagator \mathcal{D}_π contains a singularity at $T = T_M$. The leading behavior of \mathcal{D}_π can be obtained from the observation that $B_0(\sqrt{s}, \vec{0})$ can be expanded in a power series in $(4m_q^2 - s)^{1/2}$ [9]:

$$B_0(\sqrt{s}, \vec{0}) = \mathcal{A} + \mathcal{B}(4m_q^2 - s)^{1/2} + \mathcal{C}(4m_q^2 - s) + \mathcal{O}((4m_q^2 - s)^{3/2}) \quad . \quad (2.21)$$

The pion propagator can thus near threshold be approximated by

$$\mathcal{D}_\pi(\sqrt{s}, \vec{0}) = \frac{2G}{\left[1 + \xi \left(A(m_q) - 2m_q^2 \mathcal{A}\right)\right] - \frac{\xi}{2} \left[s \mathcal{B}(4m_q^2 - s)^{1/2} - (\mathcal{A} + s\mathcal{C})(4m_q^2 - s)\right]} \quad (2.22)$$

with $\xi = (N_c G)/\pi^2$. Since one has $m_\pi = 2m_q$ at $T = T_M$, the first square bracket in Eq. (2.22) has to vanish at this temperature and one obtains

$$\mathcal{D}_\pi(\sqrt{s}, \vec{0}) \sim (s - 4m_q^2)^{-1/2} . \quad (2.23)$$

Via Eqs. (B12) and (2.18), one obtains

$$\sigma_{q\bar{q} \rightarrow \gamma\gamma} \sim (s - 4m_q^2)^{-3/2} \quad (2.24)$$

near threshold. The pion propagator diagram thus leads to a strong enhancement of the production of soft photons at the Mott transition when compared with the direct contributions. Due to the temperature dependence of the pion mass (see Fig. 1) the peak in the two-photon invariant mass spectrum at $\sqrt{s} = m_\pi$ is shifted upwards to a value of $m_\pi(T_M) = 173$ MeV. Note that the effect of a rising pion mass at high temperatures is also visible in other effective models [21,22] and in lattice calculations [23]. Moreover, the $\pi^0 \rightarrow \gamma\gamma$ decay rate is strongly enhanced at the Mott transition which is an effect akin to the phenomenon of critical opalescence known from solid state physics [9]. Numerically, one finds that the resonance contributions are most pronounced near the Mott temperature, while their importance is strongly reduced compared to the direct terms at higher temperatures. A similar behaviour has been found previously in Refs. [24,25].

III. HYDRODYNAMICAL EXPANSION

The cross sections calculated in Sec. II are not measureable directly in heavy ion experiments. Instead, one has to integrate the production rates over the evolution of the system. A crude model for the expansion and cooling of the plasma has been given by Bjorken [16]. Within this model, we will use different *ansätze* for the equation of state and investigate their influence on the physical spectra.

A. Production Rates per Space–Time Element

The production rate of photon pairs with invariant mass M per unit space–time volume is given by

$$\begin{aligned} \frac{dN_{\gamma\gamma}}{d^4x dM} &= 2M \int \frac{d^3p_1}{(2\pi)^3} \frac{d^3p_2}{(2\pi)^3} v_{\text{rel}} \sigma_{\gamma\gamma}(M^2, T) \\ &\quad \times [2N_c f_F(\beta p_1^\mu u_\mu)] [2N_c f_F(\beta p_2^\mu u_\mu)] \delta(M^2 - (p_1 + p_2)^2) , \end{aligned} \quad (3.1)$$

where $f_F(x) = 1/(\exp(x) + 1)$ is the Fermi distribution function and $\sigma_{\gamma\gamma}$ the sum of the cross sections for $u\bar{u} \rightarrow \gamma\gamma$ and $d\bar{d} \rightarrow \gamma\gamma$. As in Section II, we neglect effects that stem from a relative motion of the quark pair with respect to the rest frame of the medium. In principle, Eq. (3.1) should be supplemented by Bose enhancement factors, which account for the stimulated emission of photons in the medium. Since the form of such enhancement factors is unknown and can only be determined in a nonequilibrium theory, we discard any such factors [12,13], assuming that the photon density stays low due to the short lifetime of the plasma and thus prohibiting equilibration. Note that the inclusion of an enhancement factor, even at the finally equilibrated level, only alters our results quantitatively by at most a factor of 10. Our qualitative picture remains however unchanged. The fluid velocity, which has to be supplied by the expansion model, is denoted by u_μ . As it turns out, the final result does not depend on u_μ , so one can evaluate (3.1) under the assumption that the fluid is at rest. The final result for the production rates reads [12,26]

$$\frac{dN_{\gamma\gamma}}{d^4xdM} = \frac{(2N_c)^2}{(2\pi)^4} \frac{M^2 \sqrt{M^2 - 4m_q^2} \sigma_{\gamma\gamma}(M^2, T)}{\beta} \int_{m_q}^{\infty} dE f_F(\beta E) \log \frac{1 + \exp(-\beta E_-)}{1 + \exp(-\beta E_+)} \quad (3.2)$$

with

$$E_\pm = \frac{1}{2m_q^2} \left[(M^2 - 2m_q^2)E \pm \sqrt{M^2(M^2 - 4m_q^2)(E^2 - m_q^2)} \right] \quad . \quad (3.3)$$

An expansion of Eq. (3.2) near threshold shows that the singular part of the production rate behaves as

$$\frac{dN_{\gamma\gamma}}{d^4xdM} \sim (M^2 - 4m_q^2) \sigma_{\gamma\gamma}(M^2, T) \quad . \quad (3.4)$$

At $T \neq T_M$, where $\sigma_{\gamma\gamma}$ displays only kinematical singularities, the production rate thus vanishes at threshold. At the Mott temperature, however, one obtains from Eq. (2.24), that the production rate diverges as

$$\frac{dN_{\gamma\gamma}}{d^4xdM} \sim (M^2 - 4m_q^2)^{-1/2} \quad (3.5)$$

near threshold. Note that this is an integrable singularity, i. e. although the production rate contains a divergence, the total number of photons produced stays finite.

B. Expansion Model

As a simple model for the hydrodynamical expansion, we employ Bjorkens one dimensional model [16]. The essence of this model is contained in the two equations for the fluid velocity u_μ

$$u_\mu = \frac{1}{\tau}(t, 0, 0, z) \quad (3.6)$$

and the entropy density s

$$\frac{s(\tau)}{s(\tau_0)} = \frac{\tau_0}{\tau} \quad , \quad (3.7)$$

where $\tau = \sqrt{t^2 - z^2}$ is the proper time of the fluid element. Note that all thermodynamic quantities depend on τ only. In Eq. (3.7), τ_0 denotes the formation time of the plasma, which we treat as a free parameter in the following. To compute the temperature distribution from Eq. (3.7), one has to make assumptions about the equation of state of the plasma. In the following, we will compare two different scenarios:

(i) *First order phase transition*: The entropy density changes discontinuously at $T = T_M$. In this case, the equation of state reads [14,12]

$$s = \frac{4\pi^2}{90} T^3 \times \begin{cases} d_Q & \text{if } T > T_M \\ f d_Q + (1-f) d_H & \text{if } T = T_M \\ d_H & \text{if } T < T_M \end{cases} . \quad (3.8)$$

The parameter f in Eq. (3.8) is the volume fraction of the system, which is in the quark-gluon phase, $(1-f)$ the volume fraction, which is in the hadron phase. The symbols d_i denote the effective numbers of degrees of freedom; one has $d_Q = 37$, $d_H = 3$. From Eq. (3.8), one obtains the following behavior of temperature:

1. The expansion starts at $\tau = \tau_0$ with an initial temperature T_0 . Afterwards, the temperature drops according to

$$T = T_0 \left(\frac{\tau_0}{\tau} \right)^{1/3} \quad , \quad (3.9)$$

until it reaches the Mott temperature at time

$$\tau_1 = \tau_0 \left(\frac{T_0}{T_M} \right)^3 \quad , \quad (3.10)$$

at which the mixed phase begins.

2. The second stage of the expansion is isothermal with $T = T_M$. During this stage, the relative volume of the plasma evolves according to

$$f(\tau) = \frac{1}{d_Q - d_H} \left(d_Q \frac{\tau_1}{\tau} - d_H \right) . \quad (3.11)$$

This stage ends at time

$$\tau_2 = \frac{d_Q}{d_H} \tau_1 , \quad (3.12)$$

at which $f(\tau_2) = 0$ and the system enters the purely hadronic phase.

3. During the third stage, the temperature of the system drops as

$$T = T_M \left(\frac{\tau_2}{\tau} \right)^{1/3} . \quad (3.13)$$

This stage lasts until breakup.

The solid curve of Fig. 4 gives a specific example for the parameters $T_0 = 250$ MeV and $\tau_0 = 1$ fm/c. The temperature stays constant from $\tau_1 = 1.8$ fm/c to $\tau_2 = 22.4$ fm/c.

The physical photon spectra have to be obtained by a space–time integration of the production rates. In the Bjorken model, the integration over the transverse space directions simply contributes a factor πR_A^2 , where R_A is the radius of the colliding nuclei. Since the thermodynamic quantities only depend on τ , it is useful to switch to the integration variables τ and

$$\eta = \frac{1}{2} \log \frac{t+z}{t-z} . \quad (3.14)$$

The final result is

$$\frac{dN_{\gamma\gamma}}{dM d\eta} = \pi R_A^2 \left(\int_{\tau_0}^{\tau_1} d\tau \tau \frac{dN_{\gamma\gamma}}{d^4 x dM} + \int_{\tau_1}^{\tau_2} d\tau \tau f(\tau) \frac{dN_{\gamma\gamma}}{d^4 x dM} \right) , \quad (3.15)$$

which gives the number of photons produced in the central rapidity interval of the collision. Note that Eq. (3.15) contains only contributions from the plasma phase. Although the NJL model would allow for $q\bar{q}$ annihilation in the hadronic phase, we discard these unphysical contributions by restricting the integration limits.

(ii) *Second order phase transition*: For a second order phase transition, the jump in Eq. (3.8) is smeared out over an interval ΔT according to [15]

$$s = \frac{4\pi^2}{90} T^3 \frac{d_Q - d_H}{2} \left[\frac{d_Q + d_H}{d_Q - d_H} + \tanh\left(\frac{T - T_M}{\Delta T}\right) \right] \quad . \quad (3.16)$$

In this scheme, the time evolution of the temperature has to be calculated numerically using Eq. (3.7). The result is a smooth curve, which for $\Delta T \rightarrow 0$ approaches that of the first order transition, as can be seen from the dashed ($\Delta T = 10$ MeV) and dot-dashed ($\Delta T = 1$ MeV) curves in Fig. 4. However, this scenario displays the qualitative difference to the first order scenario, that it does not develop a mixed phase. Note that for $T_0 - T_M \gg \Delta T$, the phase transition is reached at time

$$\tau_1 = \tau_0 \left(\frac{T_0}{T_M} \right)^3 \frac{2d_Q}{d_Q + d_H} \quad . \quad (3.17)$$

For the parameter set of Fig. 4, this yields $\tau_1 = 3.35$ fm/c. This is very small compared to the end time of the mixed phase in the first order scenario.

In contrast to Eq. (3.15), the photon spectrum is now given by

$$\frac{dN_{\gamma\gamma}}{dM d\eta} = \pi R_A^2 \int_{\tau_0}^{\tau_1} d\tau \tau \frac{dN_{\gamma\gamma}}{d^4 x dM} \quad . \quad (3.18)$$

As Eq. (3.15), the integration is cut off at the phase transition and thus contains only contributions of a pure quark phase.

C. Photon Spectra

The physical photon spectra at central rapidity for the case of a first order phase transition are shown in Fig. 5 as a function of the invariant pair mass. The dashed line gives the photon spectra without resonance contributions. Since the system stays at temperature $T = T_M$ for a finite time, the spectra develop a cusp at $M = 2m_q(T_M)$. The rise in the photon yield at larger pair masses reflects the contribution of the mixed phase. The photon spectra containing resonance contributions is given by the solid line in Fig. 5. Here the influence of the mixed phase is more dramatic: Due to the second term of Eq. (3.15), the threshold singularity in Eq. (3.5) immediately carries over to the physical spectra and one thus observes a great enhancement of photon pairs at the invariant mass $M = 2m_q(T_M) = m_\pi(T_M)$. For our parameter set, this occurs at $M = 173$ MeV. Note that this peak is in principle separated from the hadronic contributions due to π^0 decay ($M = 135$ MeV) and due to $\pi^+\pi^-$ annihilation ($M \geq 279$ MeV). However, we suspect that this medium

effect might hardly be visible in experiment since it is not clear if the enhancement of the pion mass is sufficient to separate the critical scattering peak from the huge peak in the photon spectra stemming from the decay of “cold pions” originating after hadronization. A quantitative estimate of the number of photon pairs originating from π^0 decay can be made from the relation [14]

$$\frac{1}{\pi R_A^2} \frac{dN_{\pi^0}}{d\eta} = 1.5 \tau_0 T_0^3 = 3.1 \text{ fm}^{-2} . \quad (3.19)$$

The total number of photon pairs contained in the solid curve of Fig. 5 is

$$\frac{1}{\pi R_A^2} \frac{dN_{\gamma\gamma}}{d\eta} = 4.0 \times 10^{-5} \text{ fm}^{-2} , \quad (3.20)$$

which is of the order of a factor α_{em}^2 less than the value given in Eq. (3.19). The number of photon pairs contained in the Mott peak is

$$\frac{1}{\pi R_A^2} \frac{dN_{\gamma\gamma}}{d\eta} = 3.8 \times 10^{-7} \text{ fm}^{-2} . \quad (3.21)$$

The Mott peak thus contains roughly 1% of the total number of photons stemming from $q\bar{q}$ annihilation.

In the case of a second order phase transition, the system does not stay at a fixed temperature for a finite time. Thus the Mott peak visible in Fig. 5 should disappear if the order of the phase transition is weakened. Figure 6 shows the effect of the parameter ΔT on the photon spectra. Here the case of the first order phase transition is shown as the solid line. The other lines show the spectra in the case of a second order phase transition for various values of ΔT . One recognizes that one still obtains a strongly enhanced photon yield at $M = m_\pi(T_M)$ for very small values of ΔT . For larger values of ΔT , however, this peak gets flattened. At $\Delta T = 20$ MeV, only a weak cusp is visible in the two-photon spectra from a quark-meson plasma.

IV. SUMMARY AND CONCLUSIONS

We have investigated the influence of resonance contributions on the process $q\bar{q} \rightarrow \gamma\gamma$ in a quark meson plasma at temperatures larger than the Mott temperature. We have employed a chiral quark model as a microscopic approach to a consistent description of the chiral phase transition and the Mott effect of the pion as a $q\bar{q}$ bound state. We have found that at the pion Mott temperature T_M ,

which corresponds to the chiral transition temperature T_χ present for $m_{0q} = 0$, there occurs a narrow peak in the two photon spectrum at the invariant mass $M = m_\pi(T_M) \approx 173$ MeV. Note that lattice results give $T_\chi = T_{\text{deconfinement}}$ within the present accuracy [23]. It seems thus natural to identify the Mott point with the deconfinement temperature.

In order to estimate the role of this critical scattering effect on the photon spectra emitted from an expanding quark plasma, as produced e. g. in heavy ion collisions, we have used the hydrodynamical Bjorken scenario. The expansion dynamics fixes the temperature near $T = T_M$ for a finite time interval, depending on the parameter ΔT of Eq. (3.16), which is a measure for the smoothness of the transition. In the case of a first order transition this leads to a divergence in the photon spectra which is, however, only of the order $(M - m_\pi(T_M))^{-1/2}$, so that the total number of photons emitted is finite. In the case of a second order phase transition, the divergence disappears. However, since the temperature stays *near* T_M for finite time, the critical scattering peak remains visible. The threshold singularity of the cross section, which is responsible for the critical scattering effect, may be weakened due to higher order corrections in $1/N_c$. We nevertheless suspect that the cross section stays large at threshold.

In the present work we have limited ourselves to the investigation of the photon pair production in the quark phase and did not take into account the contribution of the later expansion stage. This calculation is considered as a first step towards a more complete analysis of in medium effects on photon production in heavy ion collisions within chiral quark models. The hadronic tail of the evolution of a hot quark plasma phase also gives important contributions. A study of the processes in a pion gas, as $\pi^0 \rightarrow \gamma\gamma$ and $\pi^+\pi^- \rightarrow \gamma\gamma$, is in progress [27]. The applicability of quark models without confinement in the hadronic phase is limited to those kinematical situations, where unphysical quark production thresholds do not play a role. A first step towards the development of chiral confining quark models at finite temperature has been undertaken in Ref. [22]. Also in these more realistic models the Mott effect occurs and we expect its manifestation in the two photon spectra.

ACKNOWLEDGMENTS

We wish to thank J. Hüfner, S.P. Klevansky and M.K. Volkov for illuminating discussions and a careful reading of the manuscript. This work has been supported in part by the Deutsche Forschungsgemeinschaft under contracts no. 436 RUS 17/168/95 and Hu 233/4-4, and the Federal Ministry for Education and Research under contract no. 06 HD 742.

APPENDIX A: MESON TO PHOTON DECAY VERTICES

1. $\sigma \rightarrow \gamma\gamma$

The generic Feynman graph for the vertex $\sigma \rightarrow \gamma\gamma$ is given by Fig. 3 with $\Gamma = 1$. The contribution due to this diagram is

$$-iA_{\sigma \rightarrow \gamma\gamma}^{\rho\lambda} = -\frac{i}{\beta} \sum_n \int \frac{d^3q}{(2\pi)^3} \text{Tr} \left[iS_f(q) (-i\gamma^\rho q_f e) iS_f(q - k_1) iS_f(q + k_2) (-i\gamma^\lambda q_f e) \right] \quad (\text{A1})$$

where we have introduced the symbolic four vector notation

$$q = (i\omega_n, \vec{q}) \quad k_1 = (i\nu_m, \vec{k}_1) \quad k_2 = (i\alpha_l, \vec{k}_2) \quad . \quad (\text{A2})$$

In Eq. (A1), ω_n is a fermionic Matsubara frequency, whereas ν_m and α_l are bosonic Matsubara frequencies belonging to the outgoing photons. It is understood that $i\nu_m$ and $i\alpha_l$ have to be analytically continued to real values at the end of the calculation. The symbol Tr denotes the traces over spin, color and flavor degrees of freedom. Taking the trace over color and flavor yields a factor

$$N_c (q_u^2 + q_d^2) = \frac{5}{9} N_c \quad , \quad (\text{A3})$$

so that we have

$$-iA_{\sigma \rightarrow \gamma\gamma}^{\rho\lambda} = \frac{5}{9} \frac{N_c e^2}{\beta} \sum_n \int \frac{d^3q}{(2\pi)^3} \frac{\text{tr} \left[(\not{q} + m_q) \gamma^\rho (\not{q} - \not{k}_1 + m_q) (\not{q} + \not{k}_2 + m_q) \gamma^\lambda \right]}{[q^2 - m_q^2][(q - k_1)^2 - m_q^2][(q + k_2)^2 - m_q^2]} \quad , \quad (\text{A4})$$

where now the symbol tr denotes the spinor trace only. After taking the trace and noting that terms proportional to k_1^ρ and k_2^λ do not contribute to the final result due to the transversality of the photon, one has

$$-iA_{\sigma\rightarrow\gamma\gamma}^{\rho\lambda} = \frac{20}{9} \frac{N_c m_q e^2}{\beta} \sum_n \int \frac{d^3 q}{(2\pi)^3} \frac{(k_1^\lambda k_2^\rho - g^{\rho\lambda} k_1 k_2) - g^{\rho\lambda} (q^2 - m_q^2) + 4q^\rho q^\lambda}{[q^2 - m_q^2][(q - k_1)^2 - m_q^2][(q + k_2)^2 - m_q^2]} . \quad (\text{A5})$$

Decomposing this integral and performing the analytical continuation leads to

$$-iA_{\sigma\rightarrow\gamma\gamma}^{\rho\lambda} = \frac{5m_q N_c \alpha_{\text{em}}}{9\pi} (k_1^\lambda k_2^\rho - g^{\rho\lambda} k_1 k_2) \left(1 - \frac{2m_q^2}{q_1 q_2}\right) C_0(k_1, -k_2) \quad (\text{A6})$$

where $\alpha_{\text{em}} = 1/137$ is the electromagnetic fine structure constant and

$$C_0(k_1, -k_2) = \frac{16\pi^2}{\beta} \sum_n \int \frac{d^3 q}{(2\pi)^3} \frac{1}{[q^2 - m_q^2][(q - k_1)^2 - m_q^2][(q + k_2)^2 - m_q^2]} . \quad (\text{A7})$$

In the kinematical situation required throughout this work, $\vec{k}_1 = -\vec{k}_2$, $k_1^0 = k_2^0 = |\vec{k}_1| = |\vec{k}_2| = \sqrt{s}/2$, this integral can be evaluated to be [19]

$$\begin{aligned} C_0(k_1, -k_2) &= -2\mathcal{P}_0^\Lambda dp \frac{p \tanh(\beta E/2)}{E^2(s - 4E^2)} \log \left| \frac{E - p}{E + p} \right| \\ &\quad + i \frac{\pi}{s} \tanh(\beta \sqrt{s}/4) \log \left| \frac{\sqrt{s} - \sqrt{s - 4m_q^2}}{\sqrt{s} + \sqrt{s - 4m_q^2}} \right| \end{aligned} \quad (\text{A8})$$

and is thus a function of s only. Beside (A6), there is a second contribution to the vertex from the crossed diagram of Fig. 3, which arises by exchanging $k_1 \leftrightarrow k_2$ and $\rho \leftrightarrow \lambda$. The contribution of this diagram is found to be equal to that of the first diagram. The function $a(s)$ in Eq. (2.16) may be thus written as

$$-ia(s) = \frac{10m_q N_c \alpha_{\text{em}}}{9\pi} \left(1 - \frac{4m_q^2}{s}\right) C_0(k_1, -k_2) . \quad (\text{A9})$$

This result is in agreement with the result of Ref. [28].

2. $\pi^0 \rightarrow \gamma\gamma$

The vertex $\pi^0 \rightarrow \gamma\gamma$ can again be computed from Fig. 3, but now one has to take $\Gamma = i\gamma_5 \tau^3$. This leads to

$$\begin{aligned}
-iA_{\pi^0 \rightarrow \gamma\gamma}^{\rho\lambda} &= -\frac{i}{\beta} \sum_n \int \frac{d^3 q}{(2\pi)^3} \\
&\times \text{Tr} \left[iS_f(q) (-i\gamma^\rho q_f e) iS_f(q - k_1) (i\gamma_5 \tau^3) iS_f(q + k_2) (-i\gamma^\lambda q_f e) \right]
\end{aligned} \tag{A10}$$

in the same notation as in Eq. (A1). The trace over color and flavor degrees of freedom yields now

$$N_c (q_u^2 - q_d^2) = \frac{1}{3} N_c \tag{A11}$$

and one has

$$\begin{aligned}
-iA_{\pi^0 \rightarrow \gamma\gamma}^{\rho\lambda} &= \frac{i}{3} \frac{N_c e^2}{\beta} \sum_n \int \frac{d^3 q}{(2\pi)^3} \frac{\text{tr} \left[(\not{q} + m_q) \gamma^\rho (\not{q} - \not{k}_1 + m_q) \gamma_5 (\not{q} + \not{k}_2 + m_q) \gamma^\lambda \right]}{[q^2 - m_q^2][(q - k_1)^2 - m_q^2][(q + k_2)^2 - m_q^2]} \ .
\end{aligned} \tag{A12}$$

The only terms of the spinor trace which give a contribution are those, which involve γ_5 and four other gamma matrices. One obtains

$$-iA_{\pi^0 \rightarrow \gamma\gamma}^{\rho\lambda} = \frac{\alpha_{\text{em}} m_q N_c}{3\pi} \varepsilon^{\rho\lambda}{}_{\gamma\delta} k_1^\gamma k_2^\delta C_0(k_1, -k_2) \tag{A13}$$

and the same contribution from the crossed graph. In total, one has for $b(s)$ required in Eq. (2.17)

$$-ib(s) = \frac{2\alpha_{\text{em}} m_q N_c}{3\pi} C_0(k_1, -k_2) \ . \tag{A14}$$

This agrees with the result of Ref. [24].

APPENDIX B: SQUARED TRANSITION AMPLITUDES

To compute the integrated cross section, one need the square of the transition amplitude, averaged over incoming and summed over outgoing states,

$$\frac{1}{4N_c^2} \sum_{s,c} |\mathcal{M}_t + \mathcal{M}_u + \mathcal{M}_{s,\sigma} + \mathcal{M}_{s,\pi}|^2 \ . \tag{B1}$$

We will quote our results for the single terms in Eq. (B1), beginning with the t - and u -channel diagrams. For the squares of these diagrams, one has

$$\frac{1}{4N_c^2} \sum_{s,c} |\mathcal{M}_t|^2 = \frac{32\pi^2 q_f^4 \alpha_{\text{em}}^2}{N_c (t - m_q^2)^2} \left[(m_q^2 - t)(s - 2m_q^2) - (t + m_q^2)^2 \right] \tag{B2}$$

$$\frac{1}{4N_c^2} \sum_{s,c} |\mathcal{M}_u|^2 = \frac{32\pi^2 q_f^4 \alpha_{\text{em}}^2}{N_c (u - m_q^2)^2} \left[(m_q^2 - u)(s - 2m_q^2) - (u + m_q^2)^2 \right] \ , \tag{B3}$$

whereas the interference term yields

$$\frac{1}{4N_c^2} \sum_{s,c} \mathcal{M}_t \mathcal{M}_u^* = \frac{32\pi^2 q_f^4 \alpha_{\text{em}}^2}{N_c(t - m_q^2)(u - m_q^2)} m_q^2 (s - 4m_q^2) . \quad (\text{B4})$$

Performing the angular integration, one obtains

$$\begin{aligned} \int_{t_{\min}}^{t_{\max}} dt \frac{1}{4N_c} {}^2 |\mathcal{M}_t + \mathcal{M}_u|^2 &= \frac{32\pi^2 q_f^4 \alpha_{\text{em}}^2}{N_c s} \\ &\times \left[(s^2 + 4m_q^2 s - 8m_q^4) \log \frac{\sqrt{s} + \sqrt{s - 4m_q^2}}{\sqrt{s} - \sqrt{s - 4m_q^2}} \right. \\ &\quad \left. - (s + 4m_q^4) \sqrt{s(s - 4m_q^2)} \right] \end{aligned} \quad (\text{B5})$$

and from this the result for the integrated cross section *without* resonances [20].

For the squares of the s -channel diagrams, one has

$$\frac{1}{4N_c^2} \sum_{s,c} |\mathcal{M}_{s,\sigma}|^2 = \frac{1}{4N_c} s^2 (s - 4m_q^2) \left| a(s) \mathcal{D}_\sigma(\sqrt{s}, \vec{0}) \right|^2 \quad (\text{B6})$$

and

$$\frac{1}{4N_c^2} \sum_{s,c} |\mathcal{M}_{s,\pi}|^2 = \frac{1}{4N_c} s^3 \left| b(s) \mathcal{D}_\pi(\sqrt{s}, \vec{0}) \right|^2 . \quad (\text{B7})$$

The interference term of the scalar and pseudoscalar s -channels vanishes. For the interference terms of the s -channel amplitudes with the direct amplitudes, one obtains

$$\begin{aligned} \frac{1}{4N_c^2} \sum_{s,c} \mathcal{M}_{s,\sigma} \mathcal{M}_t^* &= \frac{2\pi q_f^2 \alpha_{\text{em}} m_q}{N_c} \frac{[-ia(s) \mathcal{D}_\sigma(\sqrt{s}, \vec{0})]}{t - m_q^2} \\ &\times [s(s - 4m_q^2) - (t - u)(t - m_q^2)] \end{aligned} \quad (\text{B8})$$

$$\begin{aligned} \frac{1}{4N_c^2} \sum_{s,c} \mathcal{M}_{s,\sigma} \mathcal{M}_u^* &= \frac{2\pi q_f^2 \alpha_{\text{em}} m_q}{N_c} \frac{[-ia(s) \mathcal{D}_\sigma(\sqrt{s}, \vec{0})]}{u - m_q^2} \\ &\times [s(s - 4m_q^2) - (u - t)(u - m_q^2)] \end{aligned} \quad (\text{B9})$$

for the sigma exchange and

$$\frac{1}{4N_c^2} \sum_{s,c} \mathcal{M}_{s,\pi} \mathcal{M}_t^* = \frac{2\pi \tau_{ff}^3 q_f^2 \alpha_{\text{em}} m_q}{N_c} \frac{[-ib(s) \mathcal{D}_\pi(\sqrt{s}, \vec{0})]}{t - m_q^2} s^2 \quad (\text{B10})$$

$$\frac{1}{4N_c^2} \sum_{s,c} \mathcal{M}_{s,\pi} \mathcal{M}_u^* = \frac{2\pi \tau_{ff}^3 q_f^2 \alpha_{\text{em}} m_q}{N_c} \frac{[-ib(s) \mathcal{D}_\pi(\sqrt{s}, \vec{0})]}{u - m_q^2} s^2 \quad (\text{B11})$$

for the pion exchange. Integrating over t leads to the results

$$\int_{t_{\min}}^{t_{\max}} dt \frac{1}{4N_c^2} |\mathcal{M}_{s,\sigma} + \mathcal{M}_{s,\pi}|^2 = \frac{s^2 \sqrt{s(s-4m_q^2)}}{8N_c} \left[(s-4m_q^2) \left| a(s) \mathcal{D}_\sigma(\sqrt{s}, \vec{0}) \right|^2 + s \left| b(s) \mathcal{D}_\pi(\sqrt{s}, \vec{0}) \right|^2 \right] \quad (\text{B12})$$

and

$$\begin{aligned} \int_{t_{\min}}^{t_{\max}} dt \frac{1}{4N_c^2} (\mathcal{M}_{s,\sigma} + \mathcal{M}_{s,\pi}) (\mathcal{M}_t + \mathcal{M}_u)^* = \\ -\frac{2\pi m_q q_f^2 \alpha_{\text{em}} s}{N_c} \log \frac{\sqrt{s} + \sqrt{s-4m_q^2}}{\sqrt{s} - \sqrt{s-4m_q^2}} \left[(s-4m_q^2) \left(-ia(s) \mathcal{D}_\sigma(\sqrt{s}, \vec{0}) \right) \right. \\ \left. + s \tau_{ff}^3 \left(-ib(s) \mathcal{D}_\pi(\sqrt{s}, \vec{0}) \right) \right] . \end{aligned} \quad (\text{B13})$$

From this, one immediately obtains the integrated cross section via Eq. (2.18).

REFERENCES

- [1] *Proceedings of Quark Matter '95*, Eds. A. M. Poskanzer, J. W. Harris and L. S. Schroeder, Nucl. Phys. A 590 (1995) 1c.
- [2] *Proceedings of Quark Matter '96*, Eds. P. Braun-Munzinger, H. J. Specht, R. Stock and H. Stöcker, Nucl. Phys. A 610 (1997) 1c.
- [3] M. K. Volkov, Ann. Phys. (NY) 157 (1984) 282.
- [4] U. Vogl and W. Weise, Prog. Part. Nucl. Phys. 27 (1991) 195.
- [5] S. P. Klevansky, Rev. Mod. Phys. 64 (1992) 649.
- [6] T. Hatsuda and T. Kunihiro, Phys. Rep. 247 (1994) 221.
- [7] P. Zhuang, J. Hüfner and S. P. Klevansky, Nucl. Phys. A 576 (1994) 525; W. Florkowski, J. Hüfner, S. P. Klevansky and L. Neise, Ann. Phys. (NY) 245 (1995) 445; A. Abada and J. Aichelin, Phys. Rev. Lett. 74 (1995) 3130; S. P. Klevansky, A. Ogura and J. Hüfner, *Derivation of Transport Equations for a Lagrangian with Chiral Symmetry*, Heidelberg Preprint HD-TVP-97/02 (1997); P. Rehberg and J. Hüfner, *A Numerical Study of an Expanding Plasma of Quarks in a Chiral Model*, Heidelberg Preprint HD-TVP-97/03 (1997).
- [8] P. Rehberg, S. P. Klevansky and J. Hüfner, Phys. Rev. C 53 (1996) 410.
- [9] J. Hüfner, S. P. Klevansky and P. Rehberg, Nucl. Phys. A 606 (1996) 260.
- [10] J. Dolejší, W. Florkowski and J. Hüfner, Phys. Lett. B 349 (1995) 18.
- [11] T. C. Awes for the WA80 Collaboration, in [1], p. 81c.
- [12] K. Redlich, Phys. Rev. D 36 (1987) 3378.
- [13] R. Yoshida, T. Miyazaki and M. Kadoya, Phys. Rev. D 35 (1987) 388; B. Datta, S. Raha and B. Sinha, Nucl. Phys. A 490 (1988) 733; J. Letessier and A. Tounsi, Phys. Rev. D 40 (1989) 2914; R. Baier, H. Nakagawa, A. Niégawa and K. Redlich, Phys. Rev. D 45 (1992) 4323; M. Hentschel, B. Kämpfer, O. P. Pavlenko, K. Redlich and G. Soff, *Diphoton Rates from Thermalized Matter Resulting in Ultrarelativistic Heavy Ion Collisions*, Rossendorf Preprint

FZR–142 (1996); D. K. Srivastava, B. Sinha and T. C. Awes, Phys. Lett. B 387 (1997) 21.

[14] K. Kajantie, J. I. Kapusta, L. McLerran and A. Mekjian, Phys. Rev. D 34 (1986) 2747; J. I. Kapusta, *Finite Temperature Field Theory* (Cambridge University Press, 1989).

[15] D. H. Rischke and M. Gyulassy, Nucl. Phys. A 597 (1996) 701.

[16] J. D. Bjorken, Phys. Rev. D 27 (1983) 140.

[17] E. Quack and S. P. Klevansky, Phys. Rev. C 49 (1994) 3283; J. Müller and S. P. Klevansky, Phys. Rev. C 50 (1994) 410; V. Dmitrašinović, H.-J. Schulze, R. Tegen and R. H. Lemmer, Ann. Phys. (NY) 238 (1995) 332; D. Blaschke, Yu. L. Kalinovsky, G. Röpke, S. Schmidt and M. K. Volkov, Phys. Rev. C 53 (1996) 2394.

[18] See, e.g., A. L. Fetter and J. D. Walecka, *Quantum Theory of Many Particle Systems* (McGraw–Hill, New York, 1971); A. A. Abrikosov, L. P. Gor’kov and I. E. Dzyaloshinski, *Methods of Quantum Field Theory in Statistical Physics* (Prentice–Hall, Engelwood Cliffs, N.J., 1963).

[19] P. Rehberg and S. P. Klevansky, Ann. Phys. (NY) 252 (1996) 422.

[20] L. D. Landau and E. M. Lifshitz, *Course of Theoretical Physics*, Vol. 4: *Quantum Electrodynamics* (Pergamon Press, Oxford, 1987).

[21] S. Schmidt, D. Blaschke and Yu. L. Kalinovsky, Phys. Rev. C 50 (1996) 435; Z. Phys. C 66 (1995) 85.

[22] A. Bender, D. Blaschke, Yu. L. Kalinovsky and C. D. Roberts, Phys. Rev. Lett. 77 (1996) 3724.

[23] E. Laermann in [2], p. 1c.

[24] S. P. Klevansky, Nucl. Phys. A 575 (1994) 605.

[25] D. Blaschke, M. Jaminon, Yu. L. Kalinovsky, P. Petrow, S. Schmidt and B. Van den Bossche, Nucl. Phys. A 592 (1995) 561.

[26] G. Domokos, Phys. Rev. D 28 (1983) 123; S. A. Chin, Phys. Lett. B 119 (1982)

51.

- [27] M. K. Volkov, E. A. Kuraev, D. Blaschke, G. Röpke and S. Schmidt, *Two Photon Annihilation of Pions and Compton Effect off Pions in a Hot and Dense Medium*, Rostock Preprint MPG-VT-UR 96/96, in preparation.
- [28] B. Bajc, A. H. Blin, B. Hiller, M. C. Nemes and M. Rosina, Z. Phys. A 350 (1994) 229.

FIGURES

FIG. 1. Mass spectrum of the $SU_f(2)$ NJL model. Solid line: pion mass, dashed line: double quark mass, dotted line: sigma mass.

FIG. 2. Feynman diagrams for $q\bar{q} \rightarrow \gamma\gamma$. Solid lines denote quarks, wavy lines photons and double lines mesons. Graph (a) shows the direct diagram, graph (b) the s -channel diagrams. Two more diagrams, which arise by the substitution $k_1 \leftrightarrow k_2$, $\rho \leftrightarrow \lambda$ are not shown.

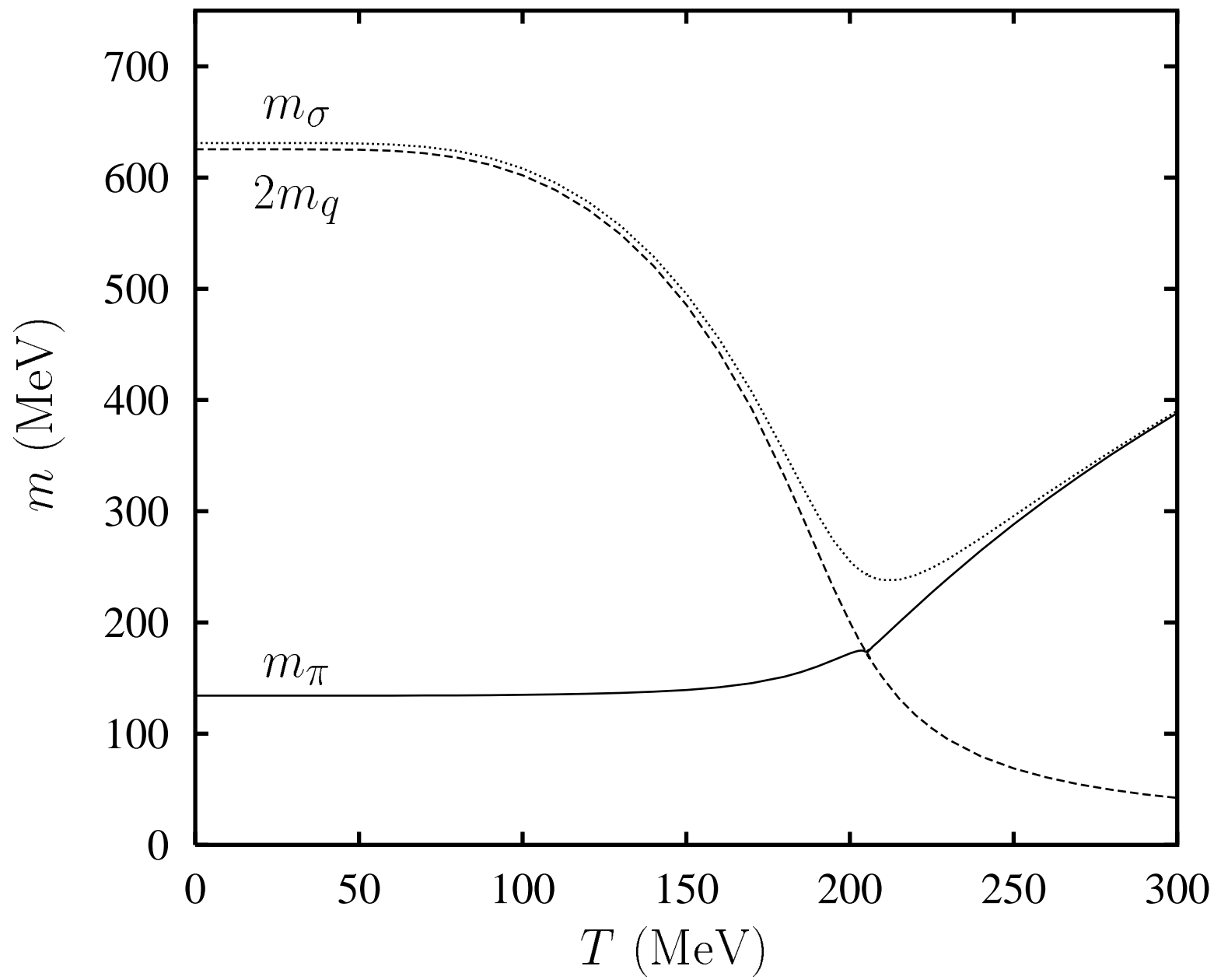
FIG. 3. Feynman diagram for the meson to photon decay vertex. Here one has to set $\Gamma = 1$ for $\sigma \rightarrow \gamma\gamma$ and $\Gamma = i\gamma_5\tau^3$ for $\pi^0 \rightarrow \gamma\gamma$. A second diagram arises by the substitution $k_1 \leftrightarrow k_2$ and $\rho \leftrightarrow \lambda$.

FIG. 4. Temperature evolution for the parameter set $T_0 = 250$ MeV and $\tau_0 = 1$ fm/ c . The solid line shows the first order scenario, the dashed and dot-dashed curves the second order scenario for $\Delta T = 10$ MeV and $\Delta T = 1$ MeV, respectively. The dotted line indicates the Mott temperature.

FIG. 5. Comparison of photon spectra containing resonance contributions (solid line) and photon spectra without resonance contributions (dashed line) in the case of a first order transition at central rapidity as a function of the invariant pair mass M .

FIG. 6. Comparison of photon spectra containing resonance contributions for a first order phase transition (solid line) and for a second order phase transition with various values of ΔT at central rapidity as a function of the invariant pair mass M .

Figure 1



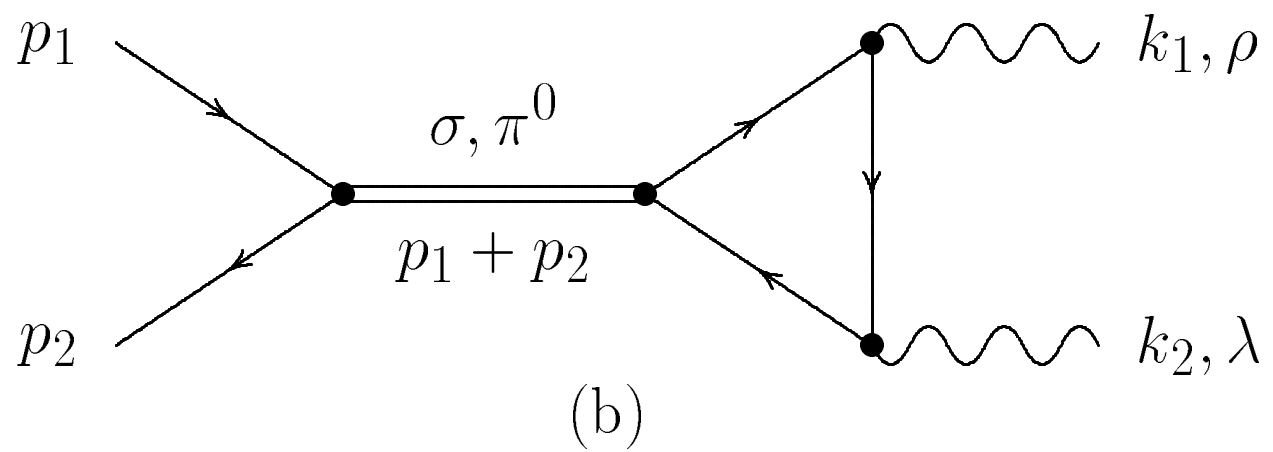
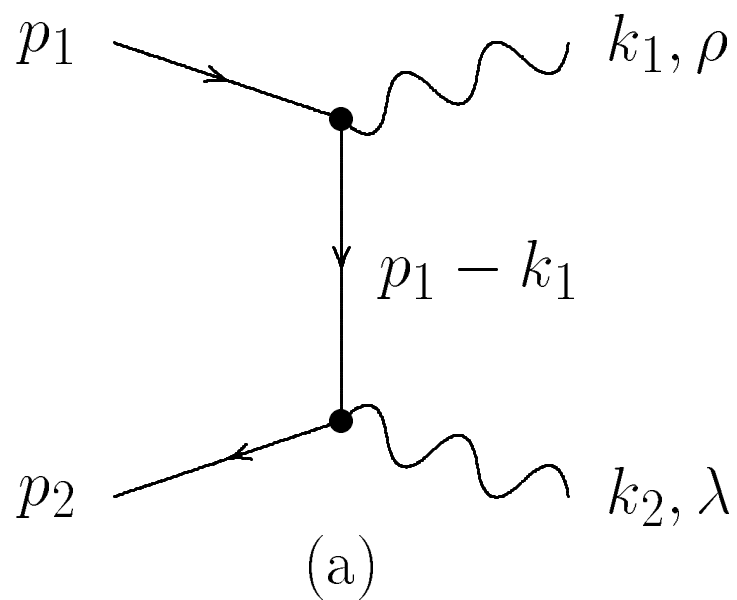


Figure 2

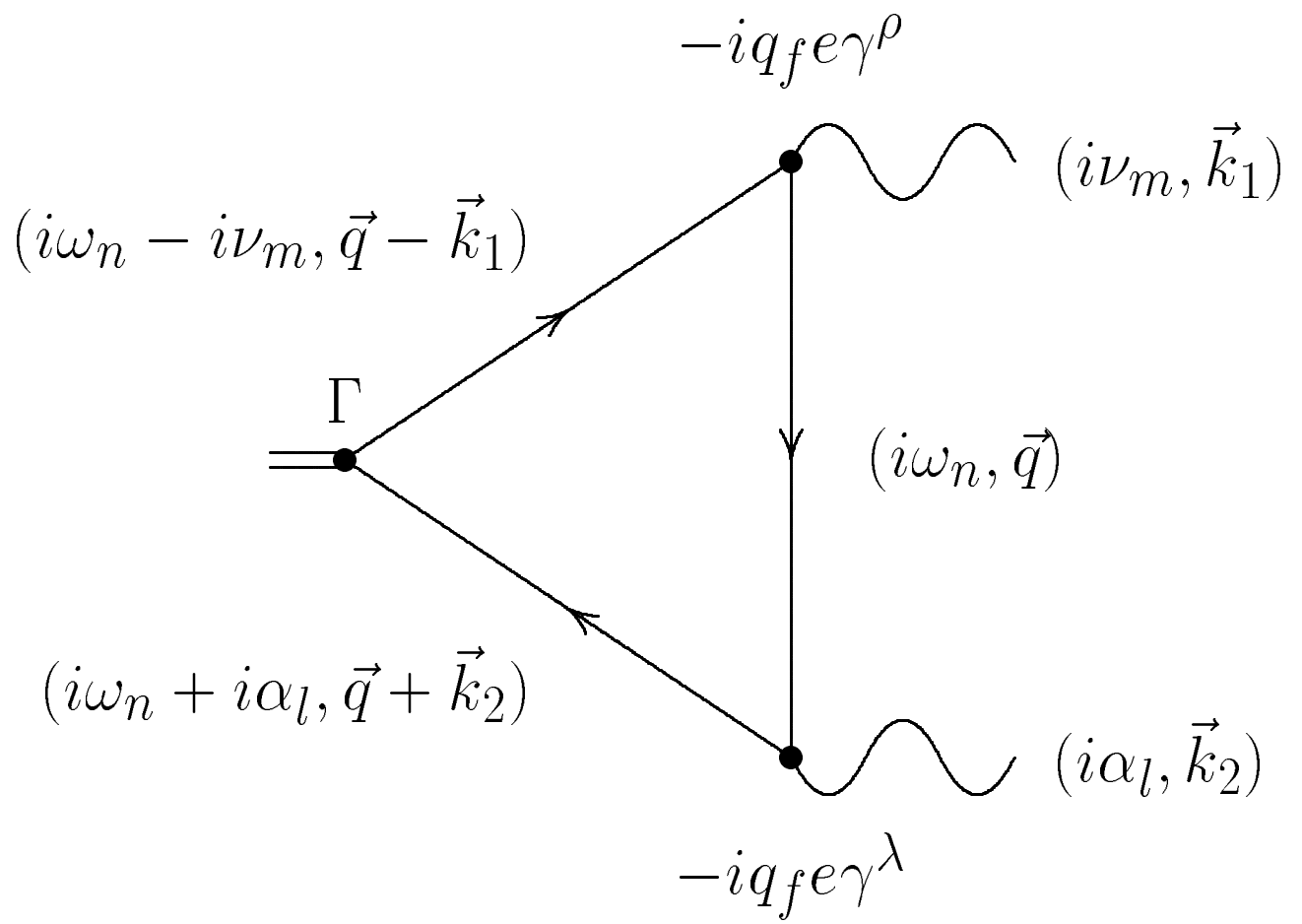
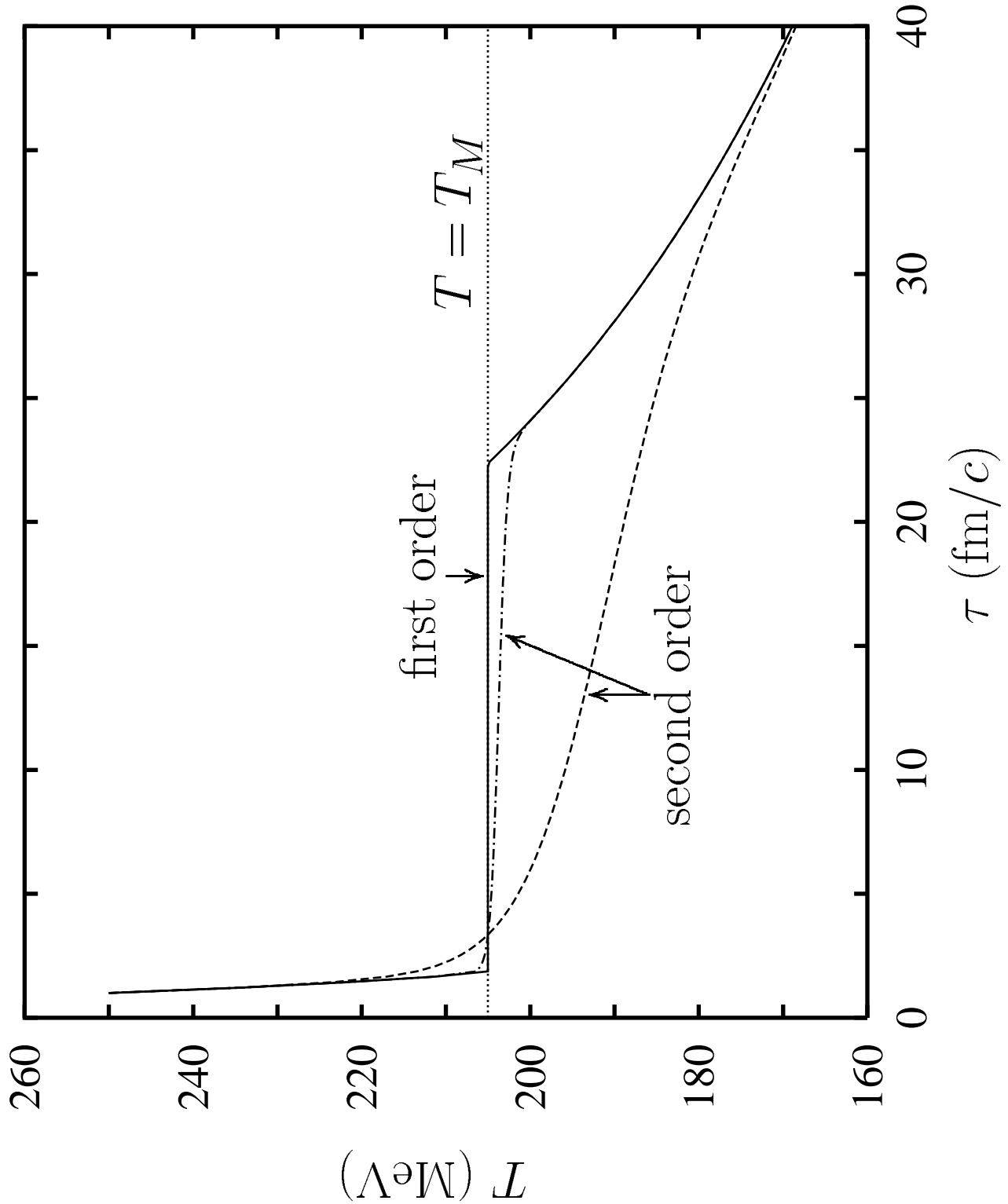


Figure 3

Figure 4



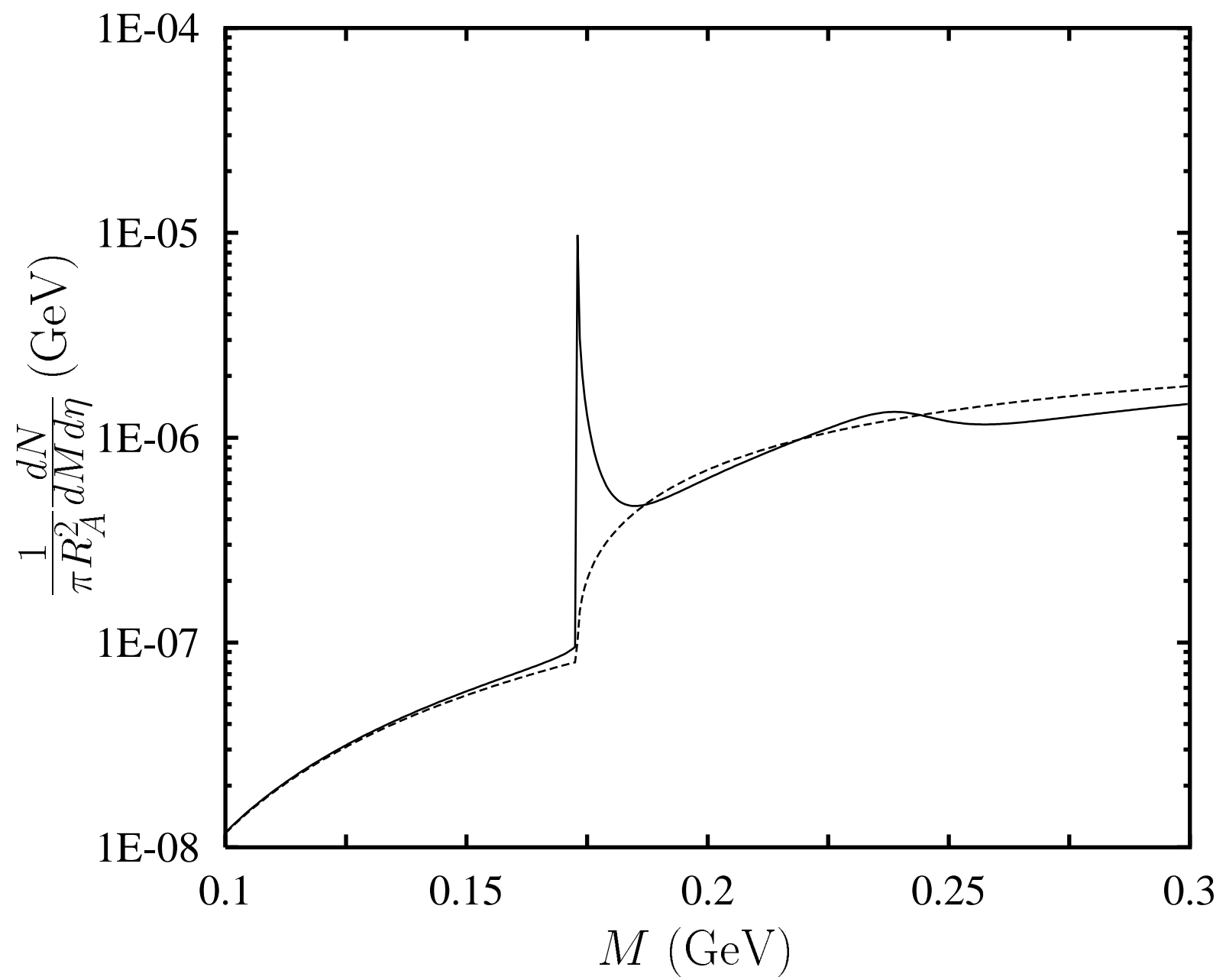


Figure 5

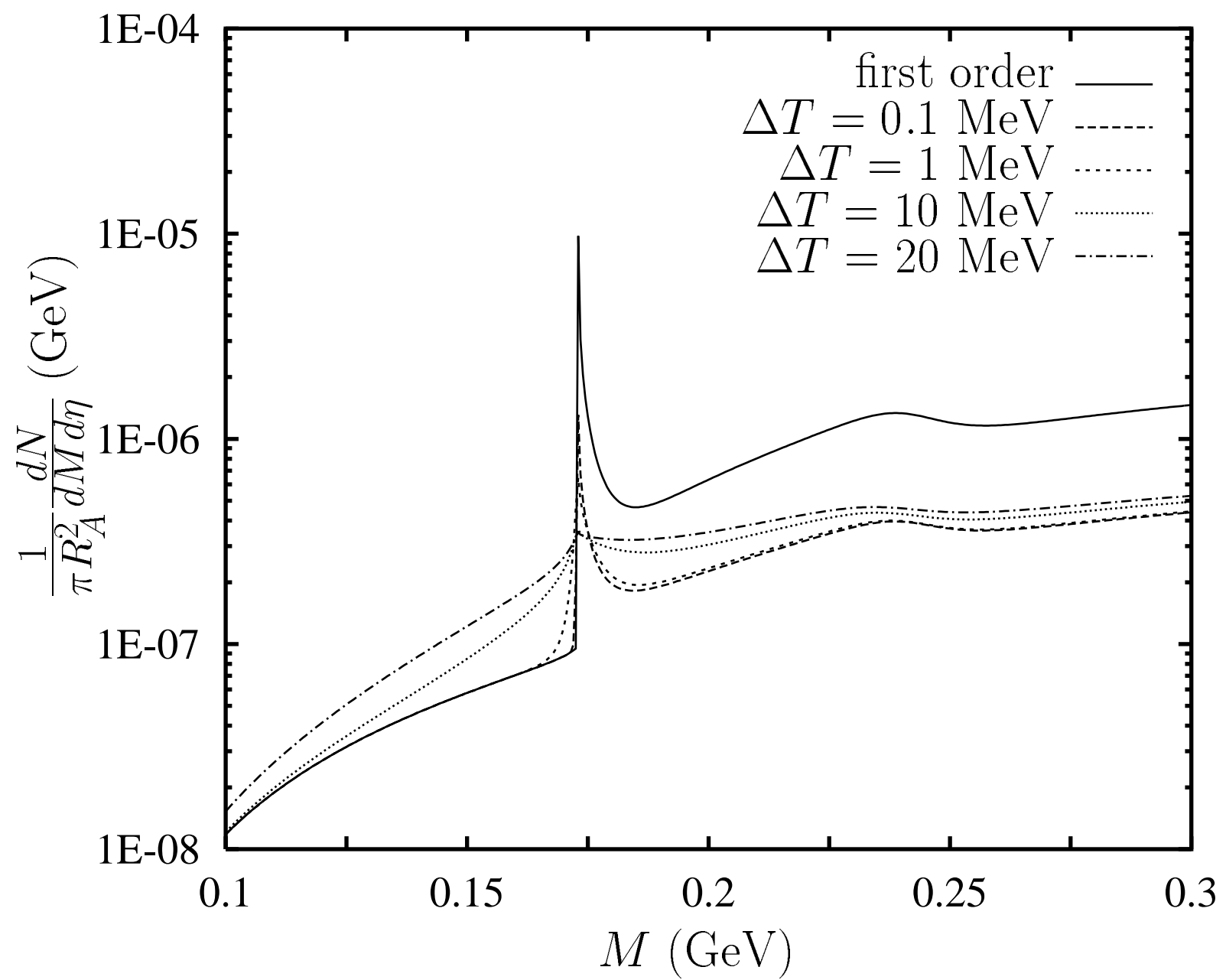


Figure 6